Electron-Transfer Activity in a Cyanide-Bridged Fe42 Nanomagnet

Michael Baker, Shu-Qi Wu, Soonchul Kang, Satoshi Matsuzawa, Marie-Anne Arrio, Yasuo Narumi, Takumi Kihara, Tetsuya Nakamura, Yoshinori Kotani, Osamu Sato, et al.

Electron Transfer Activity in a Cyanide-Bridged Fe_{42} Nanomagnet

Michael L. Baker,[*,†,‡] Shu-Qi Wu,[¶] Soonchul Kang,[§] Satoshi Matsuzawa,[‖] Marie-Anne Arrio,[⊥] Yasuo Narumi,[#] Takumi Kihara,[‖] Tetsuya Nakamura,[@] Yoshinori Kotani,[@] Osamu Sato,[*,¶] and Hiroyuki Nojiri[*,‖]

†*The School of Chemistry, The University of Manchester at Harwell, Didcot, OX11 OFA, UK.*

‡*The School of Chemistry, The University of Manchester, M139PL, Manchester, UK.*

¶*Institute for Materials Chemistry and Engineering, Kyushu University, 744 Motooka, Nishi-ku, Fukuoka, 819-0395, Japan.*

§*Department of Chemical Engineering, Graduate School of Engineering, Hiroshima University, 1-4-1, Kagamiyama, Higashihiroshima, Hiroshima, 739-8527, Japan.*

‖*Institute for Materials Research, Tohoku University, Katahira, Sendai 980-8577, Japan.*

⊥*Institut de Minéralogie, de Physique des Matériaux et de Cosmochimie, CNRS, Sorbonne Université, IRD, MNHN, UMR7590, 75252 Paris Cedex 05, France.*

#*Center of Advanced High Magnetic Field Science, Osaka University, Toyonaka 1-1, Osaka 560-0043, Japan.*

@*Japan Synchrotron Radiation Research Institute (JASRI), Sayo, Hyogo 679-5198, Japan.*

E-mail: michael.baker@manchester.ac.uk; sato@cm.kyushu-u.ac.jp; nojiri@imr.tohoku.ac.jp

Abstract

The ability to switch a molecule between different magnetic states is of considerable importance for the development of new molecular electronic devices. Desirable

properties for such applications include a large spin ground state with electronic structure that can be controlled via external stimuli. Fe_{42} is a cyanide-bridged stellated cuboctahedron of mixed valence Fe ions that exhibits an extraordinarily large S=45 spin ground state. We have found that the spin ground state of Fe_{42} can be altered by controlling humidity and temperature. Dehydration results in a 15 μB reduction of saturation magnetization that can be partially recovered on re-hydration. The complementary use of UV-vis, infrared, $L_{2,3}$-edge X-ray absorption and X-ray magnetic circular dichroism are applied to uncover the mechanism for the observed dynamic behavior. It is identified that dehydration is concurrent with metal to metal electron transfer between Fe pairs via a cyanide π hybridization. On dehydration the electron transfer occurs from low-spin $\{Fe^{II}(Tp)(CN)_3\}$ sites to high-spin Fe^{III} centers. The observed reduction in magnetization on dehydration of Fe_{42} is inconsistent with a ferrimagnetic ground state, and is proposed to originate from a change in zero field splitting at electron reduced high spin sites.

Introduction

Molecular and single chain magnets utilising cyanido-bridging ligands are of interest due to their switchable properties,[1,2] such as photo-induced magnetism,[3,4] pressure induced magnetic switching,[5] dehydration induced magnetic switching,[6] and temperature induced bi-stability of insulating (diamagnetic) phase and semiconducting (paramagnetic) phase.[7] Harnessing spin-dependent conductivity through the exploitation of such phenomena[8,9] is a strategy proposed for the realisation of molecular spintronic devices. Obtaining an atomic scale understanding of the magnetic properties of such nanoscale clusters is relevant for the development of this field. We previously reported the synthesis of Fe_{42}, a cyanide-bridged stellated cuboctahedron that exhibits an unusually large S=45 spin ground state.[10] The structure is composed of 42 cyanido-bridged iron sites that form a hollow central cavity with a diameter of 1.96 nm, Figure 1. The Fe_{42} molecule involves three unique moieties including;

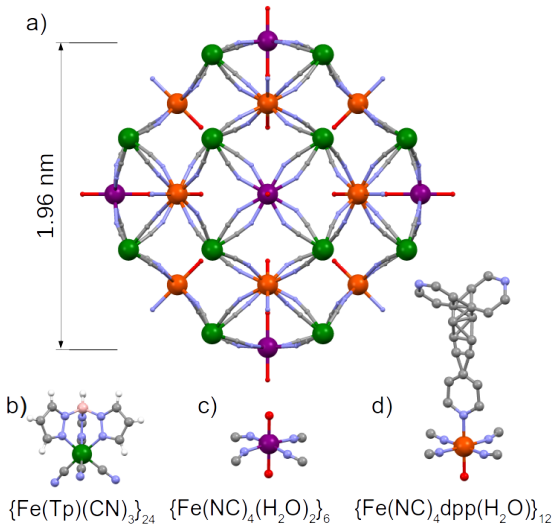

Figure 1: a) The core of the cyanide bridged Fe_{42} structure, O; red, C; grey, N; blue, Fe; green, purple and orange depending on coordination environment (hydrogen removed for clarity). The three unique Fe coordination environments; b) $\{Fe(Tp)(CN)_3\}$, c) $\{Fe(NC)_4(H_2O)_2\}$ and d) $\{Fe(NC)_4(dpp)(H_2O)\}$

24 x $\{Fe(Tp)(CN)_3\}$ (where Tp = hydrotris(pyrazolyl)borate), 6 x $\{Fe(NC)_4(H_2O)_2\}$ and 12 x $\{Fe(NC)_4(dpp)(H_2O)\}$ (where dpp = 1,3-di(4-pyridyl)propane). The S=45 spin ground state of Fe_{42} is proposed to originate from weak ferromagnetic coupling between high-spin $\{Fe^{III}(NC)_4(H_2O)_2\}$ and high-spin $\{Fe^{III}(NC)_4(dpp)(H_2O)\}$ sites.[11] These sites both terminally coordinate water molecules. In this paper we identify that the magnetism of Fe_{42} is sensitive to dehydration. Using series of spectroscopic and magnetic techniques we characterise how dehydration drives the observed changes in magnetism.

Experimental Methods

Polycrystalline samples of Fe_{42} and reference samples, were prepared as described previously.[10] The reference samples $Li[Fe^{III}(Tp)(CN)_3]$ ($Fe^{III}Tp$) and $K_2[Fe^{II}(Tp)(CN)_3]$ ($Fe^{II}Tp$) are mononuclear complexes with an equivalent coordination environment as the 24 $\{Fe(Tp)(CN)_3\}$ sites in Fe_{42}. Both complexes are six-coordinate with a facial triad of nitrogen atoms from Tp and three carbon end cyanides. Polycrystalline samples were fixed to a copper sample holder

with indium for XAS and XMCD measurements. $L_{2,3}$-edge X-ray absorption (XAS) and X-ray magnetic circular dichroism (XMCD) spectra were measured at the BL25SU beamline at SPring-8 synchrotron user facility, Japan. The monochromation of incident circularly polarised X-rays was performed using a varied line-spacing plane grating with 600 lines/mm. The $L_{2,3}$-edge measurements were performed in ultra high vacuum. Radiolysis due to X-ray overexposure was controlled by use of a shutter system reducing exposure for each incident X-ray energy to ∼200 ms. Further control of photo-reduction in Fe_{42} was enabled by attenuation of the incident photon flux to 7%. Hydration dependent XAS measurements were performed at room temperature in ultra high vacuum on BL10 at the SAGA Light Source.[12] A sample of Fe_{42} was dehydrated on a hot plate in a nitrogen atmosphere, rehydration was performed by exposing the sample to air for a few hours. The BL10 spectrometer at SAGA has a lower monochromatic energy resolution than BL25SU, consequently the SAGA spectra in Figure 8 are broader than those of Figure 6. The specific heats (see supporting information) were measured by a conventional thermal relaxation technique utilising a superconducting magnet (Oxford Instruments) at the High Field Laboratory for Superconducting Materials (HFLSM), Tohoku University. Direct current magnetic susceptibility were performed on the Quantum Design SQUID (MPMS 5S) magnetometer. To prevent the loss of water molecules, the polycrystalline Fe_{42} sample was inserted directly into the sample chamber at 100 K without purging. After keeping thermal equilibrium for several minutes and then purging the chamber, the magnetic susceptibilities were recorded from 2.0 to 400 K. The sample was kept at 400 K for 30 minutes and then pumped every 5 minutes for 30 minutes. The magnetic susceptibilities were then recorded from 400 to 2.0 K. Rehydration was performed by exposing the sample to the humid air for 3 hours. Data were corrected for the diamagnetic contribution calculated from Pascal constants. In situ dehydration was performed in the sample chamber with increasing temperature. The UV-visible reflectance spectra were performed on the MSV-350 UV/Vis microspectrophotometer (JASCO). Dehydration was performed with the commercial hot stage (Linkam) in the air. The infrared transmission spectra were

performed on the FT-IR 660 Plus spectrometer (JASCO) with a Helitran LT-3-110 system (Advanced Research Systems) to control the temperature. IR spectra were recorded using fine powder adhered to a CaF_2 plate on a JASCO FT/IR-600 Plus spectrometer in the 400 to 4000 cm^1 region. Variable-temperature IR data were collected using a helium-flow-type refrigerator (HelitranLT-3-110) with a model 331 temperature controller (LakeShore). Ligand field multiplet calculations[13] based on atomic theory,[14] including coulomb interactions[15] and spin-orbit coupling, and crystal field symmetry are used for the simulation of XAS and XMCD spectra.[16–18] $L_{2,3}$-edge XAS probes electronic transitions from the 2p core into unoccupied 3d valence orbitals, and is hence very sensitive to metal-ligand hybridization. Metal-ligand hybridization is included in the simulation of XAS spectra using the valence bond configuration interaction approach.[19] This treats both ligand to metal charge transfer (LMCT) $3d^{n+1}\underline{L}$ and metal to ligand charge transfer (MLCT) $3d^{n-1}L^-$ effects (where $\underline{L}$ and L^- correspond to a ligand with an electron hole and an extra election respectively). The charge transfer energies are defined as Δ (LMCT) and Δ^* (MLCT). The LMCT and MLCT configuration interactions are treated by hybridization terms $T_{L,i} = \langle 3d^n|h|3d^{n+1}\underline{L}\rangle$ and $T_{M,i} = \langle 3d^n|h|3d^{n-1}L^-\rangle$ respectively, where T is proportional to the overlap and h is the Hamiltonian mixing the configurations. Separate configuration T interactions are considered for e_g and t_{2g} symmetries. The calculated x-ray absorption, (left + right)/2 polarizations for SPring-8 data, and (left + right + linear)/3 polarizations for SAGA data, is normalised to the integrated intensity of the Fe_{42} data.

Experimental Results and Analysis

The influence of dehydration on UV-vis and IR spectroscopy

Dehydration, or solvent loss, induced changes in metal ion spin ground state have been observed in vacancy-type Prussian Blue analogs.[20] In such systems loss of coordinated water alters the ion ligand field resulting in a change of ion ground state that can strongly affect

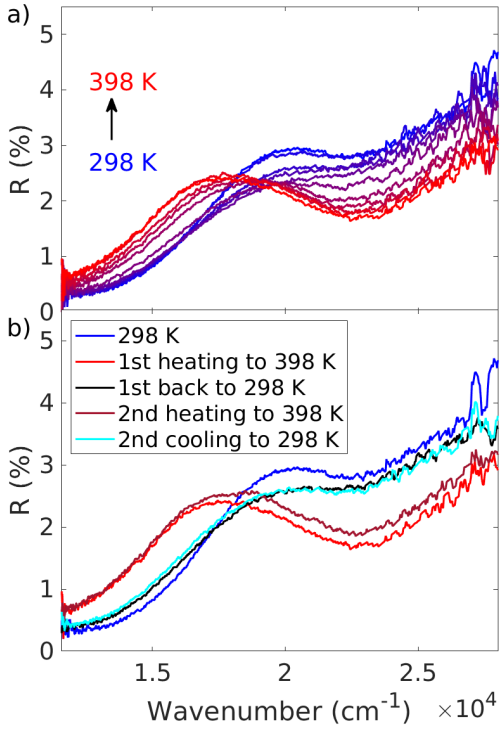

Figure 2: Solid-state UV-vis reflectance spectra of Fe_{42}, (a) measured as a function of temperature and (b) reversibility in the shifting of bands on repeated heating and cooling cycles.

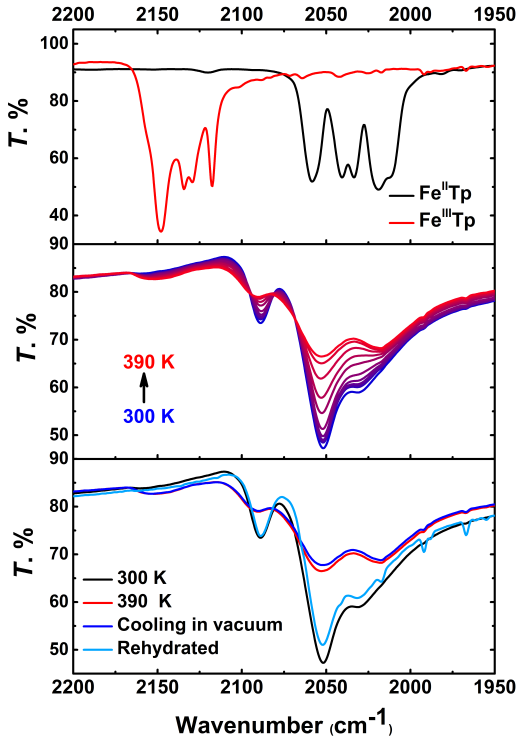

Figure 3: IR spectra for model complexes $K_2[Fe^{II}(Tp)(CN)_3]$ and $Li[Fe^{III}(Tp)(CN)_3]$ with Fe_{42} showing reversibility in spectra on cycling between both hydrated and dehydrated forms.

magnetism. Thermogravimetric analysis of Fe_{42} identifies a mass loss of approximately 5% on heating to 400 K. This reduction in mass is consistent with the loss of guest water molecules coordinated to the 18 high-spin Fe(III) sites in Fe_{42}. Following cooling to 300 K, this mass can be recovered via exposure to air (see supporting information Figure S2). Dehydration is coincident with a colour change in Fe_{42} from dark green to to dark brown. The colour of the dehydrated sample is reversed when exposed to air. The room temperature solid-state UV-Vis reflectance spectrum of Fe_{42} shows a thermally activated dehydration induced band centered at approximately 24,000 cm^{-1} that is attributed to metal-ligand charge transfer, Figure 2. A second band centred at approximately 12,000 cm^{-1} is found to decrease with increasing temperature. The solid-state measurements have a large background that inhibits clear deconvolution of the bands. However the broad lower energy band ($\sim$12,000 cm^{-1}) is consistent with the inter-valence charge transfer observed in Prussian Blue analogues.[21] Repeated heating and cooling cycles measured in air show reversibility in the absorption spectrum, Figure 2b. Cooling back to room temperature following heating, recovers the general form of the spectrum. However the bands in the recovered spectra are slightly broader than before heating.

Variable-temperature infrared (IR) spectroscopy is applied to probe for evidence of metal to metal electron transfer via changes in CN stretch modes. To aid the analysis of Fe_{42} IR spectra we start by investigating reference samples $Li[Fe^{III}(Tp)(CN)_3]$ ($Fe^{III}Tp$) and $K_2[Fe^{II}(Tp)(CN)_3]$ ($Fe^{II}Tp$). Both complexes are six coordinate with a facial triad of nitrogen atoms from Tp and three carbon end cyanides. These mononuclear clusters have an equivalent coordination environment to the 24 $\{Fe(Tp)(CN)_3\}$ sites in Fe_{42} and hence provide relevant information for the interpretation of Fe_{42}. Figure 3 shows IR spectra for $Fe^{II}Tp$ and $Fe^{III}Tp$ with Fe_{42} in both hydrated and dehydrated forms. The cyano stretching absorption bands (ν_{CN}) for $Fe^{II}Tp$ are approximately 100 cm^{-1} lower in energy than $Fe^{III}Tp$. The room temperature spectrum of Fe_{42} partially overlays with the $K_2[Fe^{II}(Tp)(CN)_3]$ spectrum and is assigned as corresponding to the bridging ν_{CN} absorption for $\{Fe^{II-LS}(\mu_{CN})Fe^{III-HS}\}$

linkages. As the temperature is increased, a new high-frequency ν_{CN} (2150 cm^{-1}) stretches are observed at a similar energy to the $Li[Fe^{III}(Tp)(CN)_3]$ ν_{CN} band. This band is hence attributed to the bridging ν_{CN} absorption of $\{Fe^{III-LS}(\mu_{CN})Fe^{II-HS}\}$ linkages. In absence of rehydration, the heated spectrum persists on cooling the sample back to 300 K and the original spectrum is partially recovered on exposure to air. The thermogravimetric analysis, UV-vis and IR results indicate that dehydration drives charge transfer in Fe_{42}.

Bulk magnetic properties

Dehydration by heating is found to significantly influence the magnetic properties of Fe_{42}. The magnetic properties of Fe_{42} before heating are consistent with our previous study[10] indicating a molecular S=45 spin ground state. In support of our previous findings we provide additional corroborating evidence for the molecular ground state of Fe_{42} via specific heat capacity measurements. The results of these measurements rule out the possibility of magnetic ordering at low temperature (see supporting information). magnetization measurements at 2.0 K as a function of applied magnetic field saturate to 90 μB at 5 T for hydrated Fe_{42}, as previously reported,[10] the magnetic field response of the dehydrated Fe_{42} does not fully saturate, with a magnetization of 75.1 μB at 5 T, Figure 4a. Figure 4b compares the temperature dependence of magnetic susceptibility for hydrated and dehydrated forms of Fe_{42}. The magnetic susceptibility of the hydrated variant of Fe_{42} increases below 10 K to a maximum of 456.6 cm^3 mol^{-1} at 2.0 K, indicating the influence of weak ferromagnetic coupling between iron spins within the molecule. Following dehydration the magnetic susceptibility shows an increase below 10 K that deviates from the hydrated variant, with a maximum of only 218.4 cm^3 mol^{-1} at 2.0 K. The χT product at 300 K remains unchanged on dehydration, at 83 cm^3 K mol^{-1} (see supporting information). Repeated heating and cooling cycles show only partial, $\sim$ 50% reversibility in the magnetic properties of Fe_{42}. In the following section we investigate the connection between the observed changes in UV-vis reflectance, IR absorption and magnetism by utilising the atomic sensitivity of XAS and XMCD.

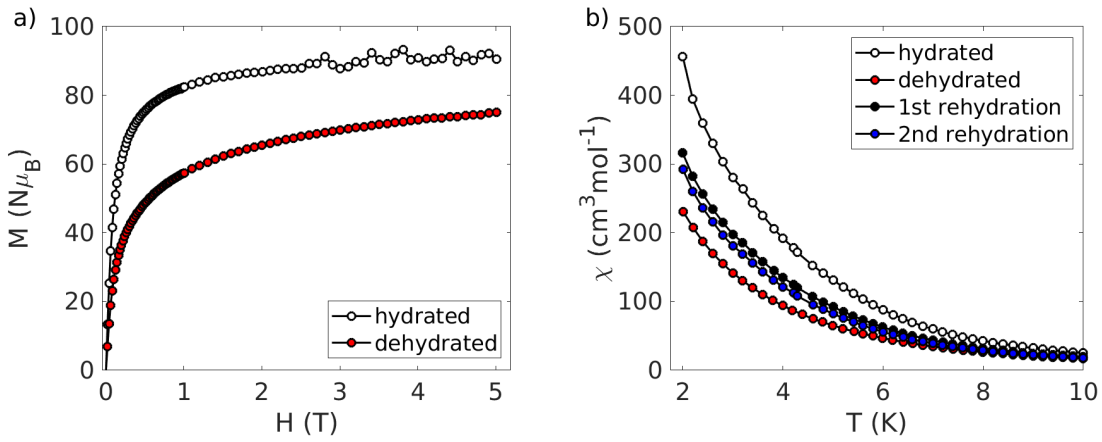

Figure 4: a) magnetization measurements of Fe_{42} in hydrated and dehydrated forms measured at 2.0 K. b) Magnetic susceptibility as a function of temperature for Fe_{42} in hydrated and dehydrated forms measured in an applied field of 50 Oe.

$L_{2,3}$-edge XAS and XMCD

Transition metal $L_{2,3}$-edge XAS and XMCD are sensitive probes of magnetism, local spin state, valence, coordination geometry and metal ligand charge transfer. Experimental access to the electronic structure of the unique Fe sites in Fe_{42} requires deconvolution of $L_{2,3}$-edge spectral contributions. To aid this process we start by investigating reference samples $Fe^{III}Tp$ and $Fe^{II}Tp$. Determining the electronic structure of the trivalent mononuclear $Fe^{III}Tp$ cluster has been the effort of several previous studies including polarised neutron diffraction,[23] $L_{2,3}$-XAS and XMCD.[22] Figure 5 shows the $L_{2,3}$-XAS of both $Fe^{III}Tp$ and $Fe^{II}Tp$. The lowest energy peak in the L_3-XAS spectrum of $Fe^{III}Tp$ (labelled with an arrow, Figure 5b) is characteristic of low-spin $3d^5$, originating from a transition into the singularly unoccupied t_{2g} hole.[24–26] The spectrum of $Fe^{II}Tp$ is consistent with a $t_{2g}^6 e_g^0$ configuration, and does not show a large low energy peak below the main L_3-edge peak. Both $Fe^{II/III}Tp$ XAS spectra show large absorptions on the high energy side of $L_{2,3}$ edges, characteristic of Fe back-donation into unoccupied CN π^* orbitals.[24] The $L_{2,3}$-edge spectra of both clusters are very similar to those of the equivalently coordinated Fe sites of the charge transfer active Co-cyanide-Fe chain, $[Co((R)-pabn)]\,[Fe(Tp)(CN)_3](BF_4)\cdot MeOH\cdot 2H_2O$[26] and dimer $[(Tp)FeIII(CN)_3CoII(PY_5Me_2)](OTf)$.[27] Charge transfer multiplet simulations of $Fe^{II}Tp$ and

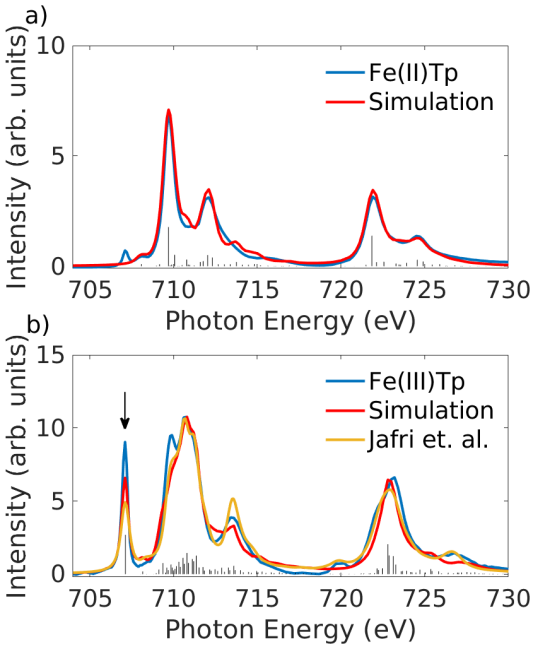

Figure 5: $L_{2,3}$-edge XAS spectra (thick solid blue lines) of $K_2[Fe^{II}(Tp)(CN)_3]$ (a) and $Li[Fe^{III}(Tp)(CN)_3]$ (b) measured at 200 K, with charge transfer multiplet simulations (red and orange solid lines). The red lines represent the result of multiplet simulation fits to XAS spectra and the vertical sticks represent the individual transition intensities. The orange line in (b) represents the results of simulations published by Jafri *et. al.* in Ref 22. The black arrow at the low energy side of the L_3 edge is characteristic of low spin $3d^5$.

$Fe^{III}Tp$ XAS spectra overlay the data in Figure 5. Simulations in Figure 5 include both LMCT and MLCT effects and are a result of trust region reflective least squares fitting to the XAS spectra(further details of the fitting procedure and a table of all the simulation parameters can be found in the supporting information). The final fits confirm that both complexes are low-spin, with considerable metal-ligand hybridization. Strongest MLCT is identified for $Fe^{II}Tp$. XAS and XMCD simulations of $Fe^{III}Tp$ were the subject of recent study reported in Ref 22. Simulations from this work are reproduced in Figure 5, labelled Jafri *et. al.*. The Jafri *et. al.* simulation includes only MLCT, and fits the XMCD data particularly well.

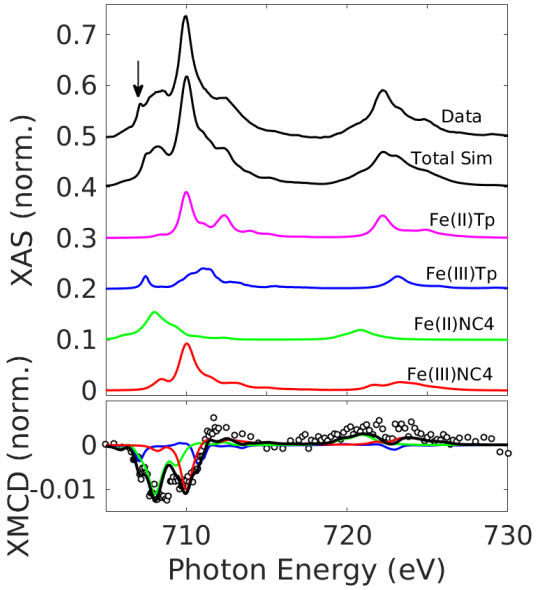

Figure 6: Top panel: The $L_{2,3}$-edge XAS ($\mu^+ + \mu^-$) of Fe_{42} (top) with charge transfer multiplet simulation and the unique components contributing to the total simulation. The black arrow labels the low energy feature that indicates the presence of $Fe^{III}Tp$. The $Fe^{II/III}Tp$ simulations are taken directly from the fits in figure 5. The $Fe^{II/III}(NC)_4$ simulations were determined by fitting to the Fe_{42} XAS and XMCD spectrum. Bottom panel: The $L_{2,3}$-edge XMCD of Fe_{42} (open circles) and charge transfer multiplet simulation (thick black line) with the contributions from 9 $Fe^{III}(NC)_4$ (green line), 9 $Fe^{II}(NC)_4$ (red line) and $Fe^{III}Tp$ (blue line). The measurements were performed at 15 K with an an applied field of 1.9 T.

The Fe_{42} L_3 and L_2 XAS intensities are distributed over a broad range of energies due to the presence of overlapping contributions from Fe moieties with different valence and

ligand field splitting, Figure 6. The XAS spectrum shows a small low energy peak (labelled with an arrow) that is consistent with $Fe^{III}Tp$ (Figure 5). This suggests that a proportion of the 24 $\{Fe(Tp)(CN)_3\}$ sites are low-spin d^5. The XMCD spectrum is dominated by high-spin Fe sites. The XMCD intensity at the L_3-edge resolves two broad negative peaks, centered at approximately 708.1 and 709.7 eV. The $L_{2,3}$-edge absorption-energy centroid of high-spin Fe^{II} ions is lower than that of high-spin Fe^{III} by 1 to 2 eV, consistent with earlier work.[28] Accordingly, the XMCD features at 708.1 and 709.7 eV originate from high-spin Fe(II) and Fe(III) magnetic species respectively. The equivalent sign of the two L_3-edge XMCD signals indicate parallel alignment of Fe^{II} and Fe^{III} spin expectation values, consistent with negligible or weak ferromagnetic exchange coupling. Detailed determination of the individual contributions from the unique moieties in Fe_{42} requires a linear combination of multiplet calculations for each of the Fe sites present. This task is simplified as the 24 $Fe^{II/III}Tp$ sites take on the parameters obtained from fitting to the reference sample spectra, leaving the contributions of 6 $\{Fe(NC)_4(H_2O)_2\}$ and 12 $\{Fe(NC)_4(dpp)(H_2O)\}$ to be determined. The coordination of $\{Fe(NC)_4(H_2O)_2\}$ and $\{Fe(NC)_4(dpp)(H_2O)\}$ (together, abbreviated as $\{Fe(NC)_4\}$) are similar, differing at one axial position by the replacement of a water with dpp (coordinated via nitrogen), for simplicity we approximate them equivalent for the simulation of Fe_{42}. The $\{Fe(NC)_4\}$ species are equatorially coordinated to four nitrogen end cyanides with frontier orbitals that mix with the Fe 3d orbitals, introducing ligand electron character into Fe molecular orbitals.[29] To account for this effect, LMCT type hybridization is included in the XAS and XMCD simulations of the high-spin sites. Initial simulations consisting of 24 low-spin $\{Fe^{II}(Tp)(CN)_3\}$ and 18 high-spin $\{Fe^{III}(NC)_4\}$, do not reproduce the double peak structure in the L_3-edge of the XMCD or the low energy side of the L_3-edge XAS (see supporting info.). The double peak structure of the XMCD and the presence of the low energy L_3-edge peak can only be reproduced by including an equal combination of 9 $\{Fe^{III}(NC)_4\}$ and 9 $\{Fe^{II}(NC)_4\}$, with 9 $\{Fe^{III}Tp\}$ and 15 $\{Fe^{II}Tp\}$. This mixed valence combination is consistent with 9 electron transfers between iron pairs

from $\{Fe^{II}Tp\}\{Fe^{III}(NC)_4\}$ to $\{Fe^{III}Tp\}\{Fe^{II}(NC)_4\}$. Figure 6 shows the Fe_{42} XAS data along with the calculated spectrum and the decomposition of contributions that give the total calculated XAS and XMCD. The free parameters in the simulation model are the $\{Fe^{II/III}(NC)_4\}$ crystal field splitting parameters and LMCT hybridization terms. Through fitting to the XMCD, the spectral contributions of the $\{Fe^{II/III}(NC)_4\}$ sites are separated out from each other and the other metal ions present in Fe_{42}. Additional details of the fitting method with a table of the final parameters are found in the supporting info.

Since the $L_{2,3}$-edge measurements are performed in an ultra-high vacuum environment partial dehydration of Fe_{42} is very probable. The effect of dehydration while heating Fe_{42} was investigated further at the $L_{2,3}$-edge at SAGA Light Source, Figure 8. Spectra measured before dehydration and after rehydration, are equivalent demonstrating reversibility in the dehydration effect. The dehydrated sample shows a clear increase in intensity centered at 708 eV. The change in XAS due to dehydration is indicative of the reduction of high-spin Fe(III) to Fe(II).[30,31] The schematic in Figure 7 outlines the basic charge transfer process, where dehydration drives a change in redox that promotes MMCT. The electron transfer process is tested against the $L_{2,3}$-edge XAS results with a linear combination of contributions according to the number of electron transfers, n, per molecule $\{Fe^{II}Tp\}_{(24\text{-}n)}\{Fe^{III}Tp\}_{(n)}\{Fe^{III}(NC)_4\}_{(18\text{-}n)}\{Fe^{II}(NC)_4\}_{(n)}$. Figure 8 shows Fe_{42} multiplet simulations for n = 9 and 12. The XAS of the hydrated Fe_{42} is reproduced with n = 9, as previously determined in the simulation of circularly polarised $L_{2,3}$-edge measurements. An electron transfer of n = 12 reproduces the observed changes in the $L_{2,3}$-edge spectrum after heating and dehydration of the sample. The reversibility of the electron transfer process observed by $L_{2,3}$-edge XAS demonstrates the necessity of heating for inducing complete charge transfer within Fe_{42} and that vacuum without heating is not sufficient.

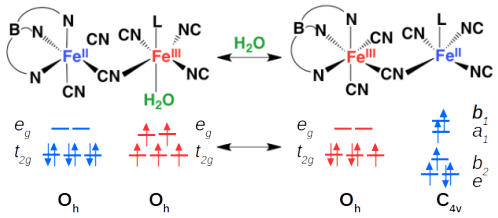

Figure 7: Schematic of the proposed dehydration induced electron transfer process between FeTp and $Fe(NC)_4$ pairs within Fe_{42}.

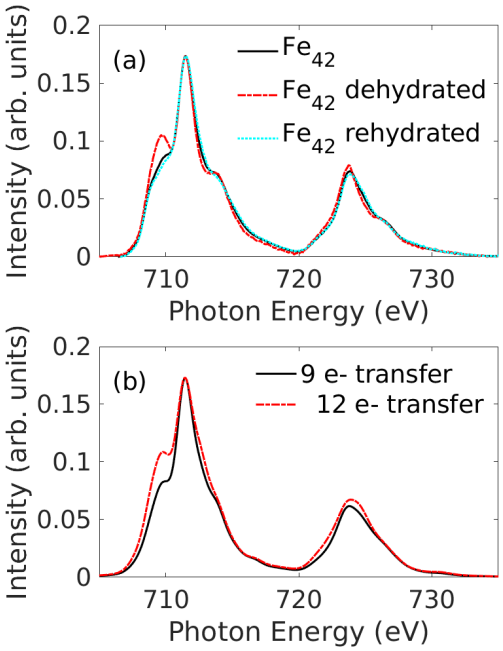

Figure 8: (a) $L_{2,3}$-edge XAS (BL10, SAGA Light Source) of Fe_{42}, Fe_{42} following dehydration and Fe_{42} after rehydration. (b) $L_{2,3}$-edge XAS simulations of the SAGA data, 9 electron transfers per Fe_{42} molecule between {FeTp} and $\{Fe(NC)_4\}$ sites reproduces the hydrated data, 12 electron transfers reproduces the dehydrated data.

Discussion

The anionic precursor $\{Fe(Tp)(CN)_3\}$ is shown to promote metal to metal electron transfer in an increasing variety of switchable coordination compounds.[32] $L_{2,3}$-edge XAS of $Fe^{II}Tp$ shows intense satellite intensity on the high energy side of both L_3 and L_2 edges characteristic for metal to ligand back-donation into π^* acceptor orbitals. Charge transfer multiplet calculations quantify this intensity as MLCT of t_{2g} electron character. In synergy with {FeTp} electron donation, Fe_{42} $L_{2,3}$-edge simulations indicate LMCT type hybridization at $\{Fe^{III}(NC)_4\}$ sites. The combined MLCT at $\{Fe^{II}Tp\}$ and LMCT at $\{Fe^{III}(NC)_4\}$ provides atomic scale evidence for the metal to metal electron transfer pathways in Fe_{42}. Prevention of water loss within Fe_{42} requires the sample to be maintained in a humid environment. It is therefore proposed that the ultra high vacuum sample environment required for $L_{2,3}$-edge measurements captures Fe_{42} in a partially dehydrated state. XMCD measurements separate the high-spin Fe(II) and Fe(III) contributions to Fe_{42}. The use of {FeTp} reference samples aids in the determination of low-spin contributions to Fe_{42}. Combined XAS and XMCD multiplet simulations identify a mixed valence Fe composition within Fe_{42} of $\{Fe^{II-LS}\}_{15}\{Fe^{III-LS}\}_9\{Fe^{III-HS}\}_9\{Fe^{II-HS}\}_9$. Further dehydration of Fe_{42} shows a clear increase of intensity in the low energy side of the L_3-edge indicating an increased contribution of high-spin Fe(II) and low spin Fe(III) to the spectrum. The observed change is due to electron transfer from $\{Fe^{II}Tp\}\{Fe^{III}(NC)_4\}$ to $\{Fe^{III}Tp\}\{Fe^{II}(NC)_4\}$. This analysis is consistent with the shift in charge transfer band observed in the temperature dependence of UV-vis spectroscopy and the temperature and dehydration dependence of μ_{CN} stretch modes identified by IR spectroscopy. The high temperature sensitivity of Fe_{42} is hence proposed to be driven by thermal dissociation of $\{Fe(NC)_4\}$ coordinated water molecules, where the resultant change redox potential invokes metal to metal electron transfer, Figure 7. The metal to metal charge transfer acts by reducing high spin sites from S=5/2 to S=2 and by oxidising low spin Fe(II) sites from S=0 to S=1/2. The number of unpaired electrons in this process remains constant, as indicated by the equivalent χT products at 300 K for both hydrated

and dehydrated samples. The magnetic susceptibility of dehydrated Fe_{42} is less than the hydrated variant below 10 K. However this reduction is inconsistent with a ferrimagnetism since the magnetic susceptibility in dehydrated Fe_{42} does not show an inflection on decreasing temperature, and the XMCD shows no evidence of strong exchange interactions between low-spin Fe(III), high-spin Fe(II) and high-spin Fe(III) sites. The loss of coordinated water molecules results in a reduction of local symmetry at $\{Fe(NC)_4\}$ sites from six coordinate (O_h) to five coordinate (C_{4v}) and potentially four coordinate (D_{4h}), in the specific case of the 6 $\{Fe(NC)_4(H_2O)_2\}$. This is consistent with $L_{2,3}$-edge simulations of $\{Fe^{II}(NC)_4\}$ sites within Fe_{42}, which requires the inclusion of a small positive D_S crystal field splitting parameter consistent with a C_{4v} distortion (see supporting info the specific parameters for the final fits). It is proposed that reduction in low temperature magnetization originates from a positive axial zero-field splitting at Fe(II) sites following water loss. In the hydrated case $\{Fe(NC)_4\}$ sites have a $^6A_1$ ground state with no evidence of zero-field splitting. Weak ferromagnetic coupling between spin sites gives rise to an isotropic S=45 molecular spin ground state. Following dehydration, $\{Fe(NC)_4\}$ sites become reduced to Fe(II) and a zero-field split S=2 single ion ground state is proposed, with sub-states, $M_S = 0, \pm 1, \pm 2$ in order of increasing energy. This zero-field splitting is transferred onto the molecular spin ground state via weak super-exchange coupling within the molecule. The energy of the zero-field splitting is small enough to be thermally populated at 10 K, as evidenced via susceptibility measurements, but is significantly larger than Fe−CN−Fe super-exchange within the Fe_{42} molecule. At temperatures lower than 10 K the $M_S = 0$ sub-state (in the uncoupled basis) is preferentially populated resulting in the observed reduction in magnetisation and lack of field induced magnetization saturation at 5 T (Figure 4).

Conclusion

The Fe_{42} molecular nanomagnet exhibits an extraordinarily large S=45 spin ground state. The discovery of charge transfer activity adds additional richness to its magnetic properties. We identify charge transfer activity driven by thermally induced dehydration. Dehydration reduces the 90 μ_B molecular saturation magnetization by 20 μ_B. Magnetic switching is partially reversible over multiple cycles. $L_{2,3}$-edge XAS and XMCD in conjunction with ligand field multiplet calculations identify that dehydration is concurrent with metal to metal electron transfer between Fe pairs via a cyanide π hybridization. The electron transfer process between pairs is identified as occurring from $\{Fe^{II}Tp\}\{Fe^{III}(NC)_4\}$ to $\{Fe^{III}Tp\}\{Fe^{II}(NC)_4\}$, this process is not coupled to a spin cross-over transition. The observed reduction in magnetization on dehydration is inconsistent with a ferrimagnetic ground state, and originates from a change in zero-field splitting at S=2 $\{Fe^{II}(NC)_4\}$ sites. Since nanoscale molecules with large molecular spin ground states are desirable for molecular spintronic applications, these results highlight the potential of harnessing metal to metal electron transfer to control the magnetic properties of large spin molecules.

Acknowledgement

The synchrotron radiation experiments were performed at the BL25SU of SPring-8 with the approval of the Japan Synchrotron Radiation Research Institute (JASRI) (Proposal No. 2013A1127) and at the beam-line BL10 of the SAGA Light Source with the approval of the Kyushu Synchrotron Light Research Center (Proposal No. 1304028PT). M. L. Baker thanks the Japanese Society for the Promotion of Science and The Royal Society of Chemistry. Grant-in-Aid for Scientific Research on Innovative Areas "Coordination programming" from the Ministry of Education, Culture, Sports, Science and Technology (MEXT). This work was supported by JSPS KAKENHI Grant Number 17H04800.

Supporting Information Available

Specific heat capacity results, thermogravimetric analysis, additional XMCD data, additional magnetization data and details regarding charge transfer multiplet calculations.

This material is available free of charge via the Internet at `http://pubs.acs.org/`.

References

(1) Sato, O.; Tao, J.; Zhang, Y.-Z. Control of Magnetic Properties through External Stimuli. *Angew. Chem. Int. Ed.* **2007**, *46*, 2152–2187.

(2) Aguila, D.; Prado, Y.; Koumousi, E. S.; Mathoniere, C.; Clerac, R. Switchable Fe/Co Prussian blue networks and molecular analogues. *Chem. Soc. Rev.* **2016**, *45*, 203–224.

(3) Sato, O.; Iyoda, T.; Fujishima, A.; Hashimoto, K. Photoinduced Magnetization of a Cobalt-Iron Cyanide. *Science* **1996**, *272*, 704–705.

(4) Mondal, A.; Li, Y.; Seuleiman, M.; Julve, M.; Toupet, L.; Buron-Le Cointe, M.; Lescouzec, R. On/Off Photoswitching in a Cyanide-Bridged Fe2Co2 Magnetic Molecular Square. *J. Am. Chem. Soc.* **2013**, *135*, 1653–1656.

(5) Coronado, E.; Giménez-López, M. C.; Korzeniak, T.; Levchenko, G.; Romero, F. M.; Segura, A.; García-Baonza, V.; Cezar, J. C.; de Groot, F. M. F.; Milner, A.; Paz-Pasternak, M. Pressure-Induced Magnetic Switching and Linkage Isomerism in K0.4Fe4[Cr(CN)6]2.816H2O: X-ray Absorption and Magnetic Circular Dichroism Studies. *J. Am. Chem. Soc.* **2008**, *130*, 15519–15532.

(6) Liu, T.; Zhang, Y.-J.; Kanegawa, S.; Sato, O. Water-Switching of Spin Transitions Induced by Metal-to-Metal Charge Transfer in a Microporous Framework. *Angew. Chem. Int. Ed.* **2010**, *49*, 8645–8648.

(7) Hoshino, N.; Iijima, F.; Newton, G. N.; Norifumi, Y.; Takuya, S.; Akiko, N.; Youichi, M.; Hiroyuki, N.; Oshio, H. Multifaceted Functionality in a Cyanide Gridged [CoFe] Chain. *Nat. Chem.* **2012**, *4*, 921–926.

(8) Aragonès, A. C.; Aravena, D.; Cerdá, J. I.; Acs-Castillo, Z.; Li, H.; Real, J. A.; Sanz, F.; Hihath, J.; Ruiz, E.; Díez-Pérez, I. Large Conductance Switching in a Single-Molecule Device through Room Temperature Spin-Dependent Transport. *Nano Lett.* **2016**, *16*, 218–226.

(9) Prins, F.; Monrabal-Capilla, M.; Osorio, E. A.; Coronado, E.; van der Zant, H. S. J. Room-Temperature Electrical Addressing of a Bistable Spin-Crossover Molecular System. *Adv. Mater.* **2011**, *23*, 1545–1549.

(10) Kang, S. et al. A ferromagnetically coupled Fe42cyanide-bridged nanocage. *Nat Commun* **2015**, *6*, 5955.

(11) Aravena, D.; Venegas-Yazigi, D.; Ruiz, E. Exchange Interactions on the Highest-Spin Reported Molecule: the Mixed-Valence Fe42 Complex. *Sci. Rep.* **2016**, *6*, 23847–.

(12) Yoshimura, D.; Setoyama, H.; Okajima, T. New Soft X-ray Beamline (BL10) at the SAGA Light Source. *AIP Conf. Proc.* **2010**, *1234*, 423–426.

(13) Thole, B. T.; van der Laan, G.; Fuggle, J. C.; Sawatzky, G. A.; Karnatak, R. C.; Esteva, J.-M. *3d* x-ray-absorption lines and the $3d^9 4f^{n+1}$ multiplets of the lanthanides. *Phys. Rev. B* **1985**, *32*, 5107–5118.

(14) Cowan, R. D. *The Theory of Atomic Structure and Spectra*; University of California Press: Berkeley, 1981.

(15) Butler, P. H. *Point Group Symmetry: Applications, Methods and Tables*; Plenum Press: New York, 1981.

(16) de Groot, F. M. F.; Fuggle, J. C.; Thole, B. T.; Sawatzky, G. A. L_2, *3* x-ray-absorption edges of d^0 compounds: K^+, Ca^{2+}, Sc^{3+}, and Ti^{4+} in O_h (octahedral) symmetry. *Phys. Rev. B* **1990**, *41*, 928–937.

(17) de Groot, F. M. F.; Fuggle, J. C.; Thole, B. T.; Sawatzky, G. A. 2 *p* x-ray absorption of 3 *d* transition-metal compounds: An atomic multiplet description including the crystal field. *Phys. Rev. B* **1990**, *42*, 5459–5468.

(18) de Groot, F. Multiplet effects in X-ray spectroscopy. *Coord. Chem. Rev.* **2005**, *249*, 31 – 63.

(19) Wasinger, E. C.; de Groot, F. M. F.; Hedman, B.; Hodgson, K. O.; Solomon, E. I. L-edge X-ray Absorption Spectroscopy of Non-Heme Iron Sites: Experimental Determination of Differential Orbital Covalency. *J. Am. Chem. Soc.* **2003**, *125*, 12894–12906.

(20) Ohkoshi, S.-i.; Arai, K.-i.; Sato, Y.; Hashimoto, K. Humidity-induced magnetization and magnetic pole inversion in a cyano-bridged metal assembly. *Nat. Mater.* **2004**, *3*, 857–861.

(21) Rogez, G.; Marvilliers, A.; Rivire, E.; Audire, J.-P.; Lloret, F.; Varret, F.; Goujon, A.; Mendenez, N.; Girerd, J.-J.; Mallah, T. A Mixed-Valence Mixed-Spin Prussian-Blue-Like Heptanuclear Complex. *Angew. Chem. Int. Ed.* **2000**, *39*, 2885–2887.

(22) Jafri, S. F.; Koumousi, E. S.; Sainctavit, P.; Juhin, A.; Schuler, V.; Bunău, O.; Mitcov, D.; Dechambenoit, P.; Mathonière, C.; Clérac, R.; Otero, E.; Ohresser, P.; Cartier dit Moulin, C.; Arrio, M.-A. Large Orbital Magnetic Moment Measured in the [TpFeIII(CN)3] Precursor of Photomagnetic Molecular Prussian Blue Analogues. *Inorg. Chem.* **2016**, *55*, 6980–6987.

(23) Karl, R.; Abhishake, M.; Corentin, B.; Olivier, C.; Béatrice, G.; Grégory, C.; Boris, L.; Karine, C.; Rodrigue, L. Polarized Neutron Diffraction to Probe Local Magnetic

Anisotropy of a Low?Spin Fe(III) Complex. *Angew. Chem. Int. Ed.* **2016**, *55*, 3963–3967.

(24) Hocking, R. K.; Wasinger, E. C.; de Groot, F. M. F.; Hodgson, K. O.; Hedman, B.; Solomon, E. I. Fe L-Edge XAS Studies of K4(Fe(CN)6) and K3(Fe(CN)6): A Direct Probe of Back-Bonding. *J. Am. Chem. Soc.* **2006**, *128*, 10442–10451.

(25) Hocking, R. K.; Wasinger, E. C.; Yan, Y.-L.; deGroot, F. M. F.; Walker, F. A.; Hodgson, K. O.; Hedman, B.; Solomon, E. I. Fe L-Edge X-ray Absorption Spectroscopy of Low-Spin Heme Relative to Non-heme Fe Complexes:? Delocalization of Fe d-Electrons into the Porphyrin Ligand. *J. Am. Chem. Soc.* **2007**, *129*, 113–125.

(26) Baker, M. L.; Kitagawa, Y.; Nakamura, T.; Tazoe, K.; Narumi, Y.; Kotani, Y.; Iijima, F.; Newton, G. N.; Okumura, M.; Oshio, H.; Nojiri, H. X-ray Magnetic Circular Dichroism Investigation of the Electron Transfer Phenomena Responsible for Magnetic Switching in a Cyanide-Bridged [CoFe] Chain. *Inorg. Chem.* **2013**, *52*, 13956–13962.

(27) Jafri, S. F. et al. Atomic Scale Evidence of the Switching Mechanism in a Photomagnetic CoFe Dinuclear Prussian Blue Analogue. *J. Am. Chem. Soc.* **2019**, *141*, 3470–3479.

(28) Kowalska, J. K.; Nayyar, B.; Rees, J. A.; Schiewer, C. E.; Lee, S. C.; Kovacs, J. A.; Meyer, F.; Weyhermüller, T.; Otero, E.; DeBeer, S. Iron L2,3-Edge X-ray Absorption and X-ray Magnetic Circular Dichroism Studies of Molecular Iron Complexes with Relevance to the FeMoco and FeVco Active Sites of Nitrogenase. *Inorg. Chem.* **2017**, *56*, 8147–8158.

(29) Arrio, M.-A.; Sainctavit, P.; Cartier dit Moulin, C.; Mallah, T.; Verdaguer, M.; Pellegrin, E.; Chen, C. T. Characterization of Chemical Bonds in Bimetallic Cyanides Using X-ray Absorption Spectroscopy at L2,3 Edges. *J. Am. Chem. Soc.* **1996**, *118*, 6422–6427.

(30) Kuepper, K.; Derks, C.; Taubitz, C.; Prinz, M.; Joly, L.; Kappler, J.-P.; Postnikov, A.; Yang, W.; Kuznetsova, T. V.; Wiedwald, U.; Ziemann, P.; Neumann, M. Electronic structure and soft-X-ray-induced photoreduction studies of iron-based magnetic polyoxometalates of type (M)M512FeIII30 (M = MoVI, WVI). *Dalton Trans.* **2013**, *42*, 7924–7935.

(31) Kuepper, K.; Taubitz, C.; Taubitz, D.; Wiedwald, U.; Scheurer, A.; Sperner, S.; Saalfrank, R. W.; Kappler, J.-P.; Joly, L.; Ziemann, P.; Neumann, M. Magnetic Ground-State and Systematic X-ray Photoreduction Studies of an Iron-Based Star-Shaped Complex. *J. Phys. Chem. C.* **2011**, *2*, 1491–1496.

(32) Mathoniere, C. Metal-to-Metal Electron Transfer: A Powerful Tool for the Design of Switchable Coordination Compounds. *Eur. J. Inorg. Chem.* **2018**, 248–258.

Graphical TOC Entry

Dehydration driven metal to metal electron transfer is identified for Fe_{42}, a molecular cluster with a S=45 ground state. The switching process is partially recoverable and results in a reduction of saturation magnetization. This process is identified by X-ray magnetic circular dichroism.